https://doi.org/10.5194/egusphere-2026-1904
Preprint. Discussion started: 10 June 2026

Integrating propagation and recovery dynamics into groundwater drought vulnerability assessment through exposure, pressure, and aquifer system response.

Katarzyna Sawicka[1], Klaudia Jurzyk[1]

[1]Faculty of Geology, University of Warsaw, Żwirki i Wigury Street, 93, 02-089 Warsaw, Poland

Correspondence to: Katarzyna Sawicka (sawicka@uw.edu.pl)

Abstract. Groundwater drought is influenced more by system-specific response dynamics than by meteorological forcing alone. We introduce a multi-scale framework that combines exposure, pressure, and sensitivity with process-based metrics of drought propagation and recovery to assess groundwater drought vulnerability. The Drought Impact Potential Index (DIPI) is developed and tested across a regional aquifer system. Propagation probability, median recovery time, and resilience metrics are examined across temporal scales and in groundwater systems at different depths. The findings reveal that spatial vulnerability patterns are driven by variations in system memory and response time. Deeper aquifer systems tend to have higher propagation probability, longer recovery periods, and increased vulnerability, indicating delayed responses and persistent drought signals. Conversely, shallower systems respond more quickly and recover faster, leading to lower drought persistence. The spatial distribution of DIPI remains consistent whether using weighted or unweighted versions, confirming that the identified patterns are robust and reflect fundamental hydrogeological controls. These results demonstrate that groundwater drought vulnerability arises from interactions between external forcing and internal system dynamics and cannot be understood solely through static indicators. An area-based analysis of exposure–pressure contrast shows that 60.4% of the study area is dominated by the intrinsic system response, compared to 21.8% driven primarily by human pressure. The proposed framework offers a process-based approach for groundwater drought assessment and can be applied to other diverse aquifer systems.

1 Introduction

Groundwater drought is increasingly recognized as a critical component of hydrological extremes, with impacts extending beyond water supply to ecosystems and water-dependent sectors. Unlike meteorological drought, groundwater drought reflects the integrated response of subsurface storage and flow processes, typically exhibiting delayed onset, attenuation of short-term variability, and prolonged persistence (Van Loon, 2015; Bloomfield & Marchant, 2013). As a result, groundwater drought cannot be interpreted as a direct response to precipitation deficits, but must be understood in the context of aquifer properties, recharge processes, and system memory.

https://doi.org/10.5194/egusphere-2026-1904
Preprint. Discussion started: 10 June 2026

Previous studies have demonstrated that the propagation of meteorological drought into groundwater is highly variable and strongly controlled by hydrogeological conditions, including storage capacity, hydraulic connectivity, and recharge mechanisms (Barker et al., 2016; Bloomfield et al., 2019). Groundwater systems generally exhibit the longest and most complex response times within the hydrological cycle, reflecting the cumulative nature of subsurface processes and delayed transmission of climatic signals (Zhu et al., 2022; Teutschbein et al., 2025). In particular, deeper and more confined aquifers tend to filter short-term variability and respond primarily to prolonged forcing, whereas shallow systems remain more directly coupled to atmospheric conditions.

A key feature of groundwater drought is the asymmetry between propagation and recovery processes. While propagation depends on the accumulation of meteorological deficits, recovery requires sustained recharge and is therefore typically slower and more constrained, particularly in systems with high storage capacity (Van Loon et al., 2016; Thomas & Famiglietti, 2017). This asymmetry leads to persistent groundwater deficits even after meteorological conditions improve, explaining the decoupling between meteorological and groundwater drought signals observed in many regions.

In human-modified environments, groundwater drought dynamics are further influenced by anthropogenic pressures such as groundwater abstraction and mining-related dewatering, which alter hydraulic gradients and storage conditions (Van Loon et al., 2016). Recent studies indicate that groundwater drought may be driven either by climatic forcing or by human activities, depending on local conditions, with anthropogenic impacts often amplifying drought severity, duration, and recovery time (Gleeson et al., 2020; Jiao D. et al., 2020; Ghasempour et al., 2025). However, these effects are spatially heterogeneous and interact with intrinsic aquifer properties, making it difficult to disentangle the relative contribution of external forcing and internal system response.

Despite substantial progress in groundwater drought research, existing approaches typically focus either on temporal dynamics (e.g., propagation and recovery analysis) or on spatial vulnerability assessment using composite indices. These perspectives are rarely integrated into a unified framework that explicitly links process-based system behavior with spatial patterns of drought impact. Moreover, widely used groundwater vulnerability frameworks are typically based on static indicators and expert-based weighting schemes, which, despite their practical applicability, do not explicitly represent process-based dynamics such as delayed recovery, threshold-type propagation, and system memory effects (Ling et al., 2023; Saha et al., 2021). In contrast, process-based approaches explicitly account for the temporal dynamics of groundwater systems, linking drought propagation and recovery to aquifer properties and system memory, thereby providing a more physically grounded basis for assessing groundwater drought vulnerability.

This study addresses this gap by developing a process-oriented framework that integrates groundwater drought dynamics with spatial assessment of impact potential. We introduce a composite Drought Impact Potential Index (DIPI) that combines exposure, pressure, and system sensitivity and explicitly incorporates process-based metrics derived from groundwater drought characteristics. In addition, we propose a spatial contrast approach based on the difference between exposure and pressure (E − P), which enables disentangling the relative influence of intrinsic system response and anthropogenic forcing on the spatial distribution of groundwater drought impact.

https://doi.org/10.5194/egusphere-2026-1904
Preprint. Discussion started: 10 June 2026

The objectives of this study are to: (1) quantify groundwater drought dynamics across multiple temporal scales using standardized indices, (2) evaluate differences in propagation and recovery behavior between aquifer systems with contrasting hydrogeological characteristics, and (3) assess the spatial distribution of groundwater drought impact potential by integrating exposure, pressure, and sensitivity components. By linking temporal drought dynamics with spatial vulnerability patterns, this study provides a mechanistic basis for understanding groundwater drought in complex, human-impacted aquifer systems.

2 Study area

2.1 Location and general setting

The study was conducted within Groundwater Body No. 43 (PLGW600043; hereafter GWB 43), located in the Odra basin and extending across northern Greater Poland and parts of Kuyavia (Fig. 1). The unit covers approximately 3,666 km² and consists of a mosaic of agricultural landscapes, lake basins, and river valleys shaped by Late Pleistocene glaciations. The area features low relief, extensive sandy plains, and numerous depressions that promote groundwater–surface water interactions (GWB 43 status card, 2022).

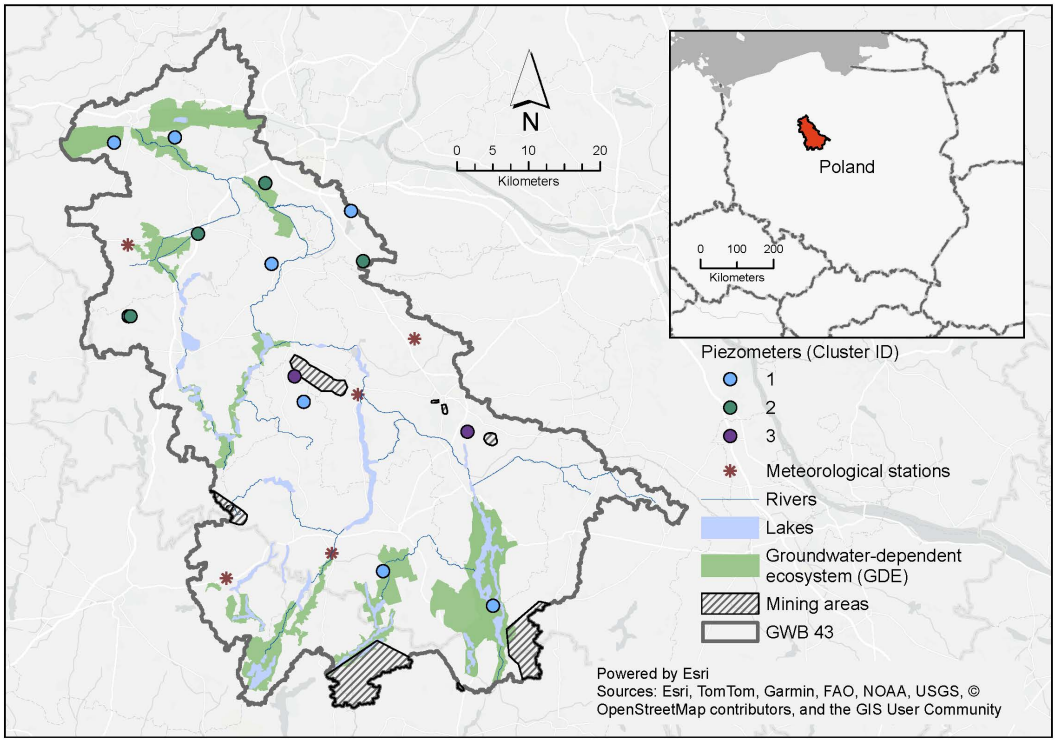

Figure 1: Study area and monitoring network within GWB 43. Location of GWB 43 (PLGW600043) in central-western Poland and spatial distribution of monitoring piezometers grouped into three aquifer systems. The figure includes hydrographic features, lakes, groundwater-dependent ecosystems (GDEs), and mining areas used in the spatial drought-impact framework.

https://doi.org/10.5194/egusphere-2026-1904
Preprint. Discussion started: 10 June 2026

2.2 Hydrogeological framework

GWB 43 comprises three principal aquifer systems: (1) shallow Quaternary sands and gravels, (2) Neogene–Paleogene sandy formations associated with lignite-bearing sequences, and (3) locally fractured Upper Cretaceous carbonates. Recharge of the shallow system occurs mainly through direct infiltration of precipitation, whereas the deeper aquifers are replenished by leakage through discontinuous clay layers and via hydraulic windows. Strong vertical connectivity between aquifers has been documented in several zones, particularly where mining drainage or river valleys modify the hydraulic gradient. This structural configuration results in a system that is sensitive to both climatic forcing and anthropogenic drainage (GWB 43 status card, 2022).

Since 2012, national assessments have consistently classified GWB 43 as having poor quantitative and chemical status. Exceedances most often involve nitrate, ammonium, sulfate, and sodium, reflecting the combined impact of agricultural runoff, inadequate rural sanitation, and possible upconing of mineralized waters from deeper layers. Many monitoring wells lack protective low-permeability covers, further increasing their vulnerability to pollution and speeding up the transfer of surface signals into groundwater (The Polish Geological Institute - National Research Institute, 2022). These features are illustrated in the conceptual cross-section (Fig. 2).

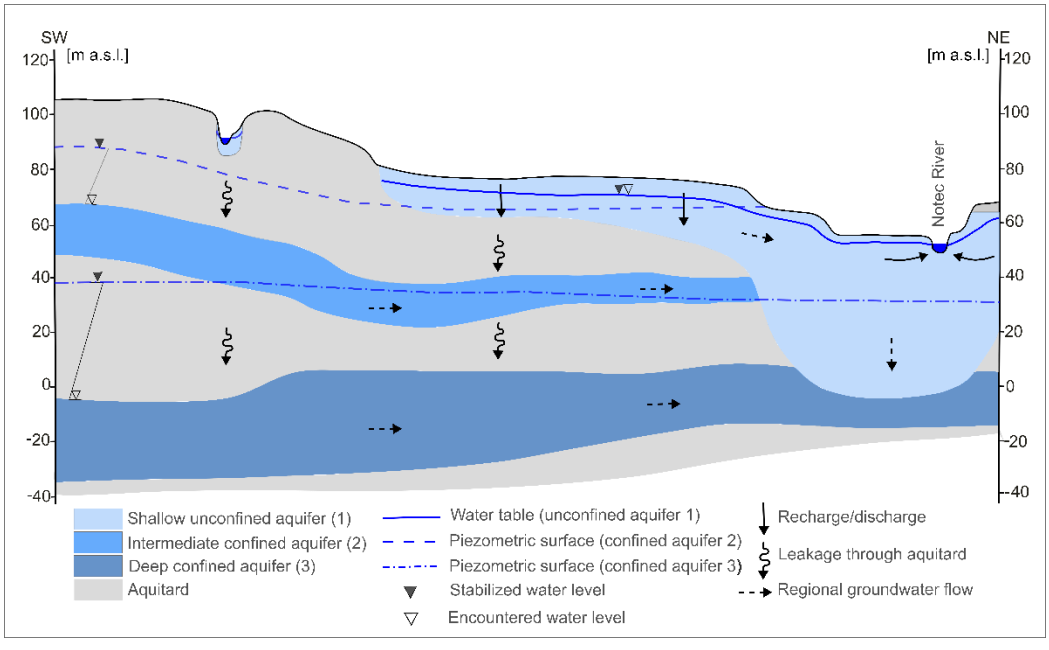

Figure 2: Conceptual hydrogeological cross-section of the GWB 43 aquifer system. Conceptual SW–NE cross-section illustrating the three principal aquifer systems in GWB 43: shallow unconfined, intermediate confined, and deep confined aquifers. The scheme highlights vertical hydraulic connectivity, leakage through aquitards, recharge/discharge zones, and dominant regional groundwater-flow directions that underpin differences in drought propagation and recovery

https://doi.org/10.5194/egusphere-2026-1904
Preprint. Discussion started: 10 June 2026

2.3 Anthropogenic pressures on groundwater systems

The groundwater system within GWB 43 faces significant human-induced stress from both groundwater extraction and mining activities. Based on available data, a total of 1267 groundwater-related features were identified in the study area, including 1247 abstraction wells and 20 dewatering wells linked to mining operations. The spatial distribution of groundwater abstractions and mining activities, along with the normalized pressure layers used in the DIPI framework, is shown in Appendix A (Fig. A1).

Groundwater abstraction is widespread and includes a range of uses, such as municipal water supply, agricultural abstraction, and individual wells serving local infrastructure (e.g., schools, healthcare facilities, and dispersed settlements). The spatial distribution of these wells is heterogeneous, with locally high densities reflecting areas of intensified water use.

In addition to abstraction, groundwater conditions are influenced by mining-related dewatering associated with open-pit operations. These activities generate local-to-regional-scale depression cones and modify hydraulic gradients, thereby affecting groundwater flow patterns and storage conditions (Fiszer, Derkowska-Sitarz, 2010; Przybyłek, 2018; Nowak et al., 2023).

The coexistence of widespread groundwater abstraction and localized high-intensity dewatering results in a complex pattern of anthropogenic pressure superimposed on natural hydrogeological conditions. This makes GWB 43 a representative example of a groundwater system where climatic forcing interacts with substantial human pressure, providing a suitable framework for analyzing the combined effects of system response and external stressors on groundwater drought dynamics.

The spatial distribution of these anthropogenic pressures is synthesized in the pressure component (P) and presented as a continuous surface in Fig. 6, forming one of the key inputs to the DIPI framework.

3 Datasets

This study integrates groundwater-level, groundwater-chemistry, and precipitation datasets for the GWB 43 groundwater body. The objective was to characterize groundwater drought dynamics consistently across aquifer levels and to compare them with meteorological forcing.

3.1. Precipitation

Monthly precipitation totals were obtained from five meteorological stations operated by the Institute of Meteorology and Water Management – National Research Institute (IMGW-PIB): Gębice, Zalesie, Trzemeszno, Pakość and Jaksice. Continuous records covering 1986–2024 were used to compute the Standardized Precipitation Index (SPI) at monthly resolution, consistent with SGI calculations.

3.2. Groundwater

https://doi.org/10.5194/egusphere-2026-1904
Preprint. Discussion started: 10 June 2026

Groundwater-level records were obtained from the national monitoring network operated by the Polish Geological Institute – National Research Institute (Państwowy Instytut Geologiczny – Państwowy Instytut Badawczy; PIG-PIB) under the State Hydrogeological Service (Państwowa Służba Hydrogeologiczna; PSH), and by the Chief Inspectorate of Environmental Protection (Główny Inspektorat Ochrony Środowiska; GIOŚ) within the State Environmental Monitoring program (Państwowy Monitoring Środowiska; PMŚ). The hydrogeological and meteorological time series used in this study were partly derived from raw datasets compiled in an earlier MSc thesis focused on a preliminary groundwater drought assessment in GWB 43 (Jurzyk, 2025). In the present study, however, these input data were reprocessed within a substantially revised analytical framework, including a new expert-based piezometer classification, expanded event-based drought metrics, and the development of the Drought Impact and Pressure Index (DIPI). Sixteen monitoring wells within GWB 43 were selected and assigned to three hydrostratigraphic groups: unconfined, intermediate, and deep confined aquifers. Hydraulic heads were converted to monthly means and used to compute the Standardized Groundwater Level Index (SGI).

Key characteristics of the groundwater monitoring wells aggregated by aquifer type are summarised in Table 1. Observation periods differ among wells; therefore, period limits refer to the earliest and latest observations available within each cluster.

Table 1: Characteristics of monitoring piezometers grouped by aquifer system in GWB 43.

Aquifer	Piezometers	Mean water-table depth (m b.g.l.)	Mean interval thickness (top–bottom, m b.g.l.)	Observation period
1 — shallow unconfined	II/906/1, II/908/1, II/908/2, II/1271/1, II/1272/1, II/1273/1, II/1274/1, II/1274/2, II/1276/1, II/1285/1	5.9	5.9–17.3	2005–2021
2 — intermediate confined	II/521/1, II/527/1, II/1272/2, II/1275/1	16.3	16.3–28.3	1986–2024
3 — deep confined	II/797/1, II/1065/1	68.0	68.0–83.0	1991–2024

The assignment of piezometers to three hydrogeological groups was defined a priori, based on stratigraphic position, confinement conditions, and typical groundwater-table depth. These groups represent conceptually distinct groundwater systems (unconfined, confined, intermediate, and deep confined). The stability of SGI responses across 3-, 6-, and 12-month aggregations indicates that the observed differences are linked to storage capacity and recharge connectivity, rather than to artefacts of temporal averaging.

https://doi.org/10.5194/egusphere-2026-1904
Preprint. Discussion started: 10 June 2026

Since the grouping is expert-based rather than statistical analysis, and the number of observation wells in confined horizons is limited (4 and 2 wells, respectively), the results should be viewed as characteristic of typical settings rather than as population-wide statistics for the entire aquifer. This limitation is somewhat offset by the internal consistency of SGI metrics across different indices and by agreement with the conceptual hydrogeological model. Future work should evaluate the stability of these groups with additional monitoring points and, where possible, use complementary statistical grouping methods.

4. Methods

The conceptual model highlights differences in damping, lag and memory effects, which are quantified using the drought metrics described below (Fig. 3).

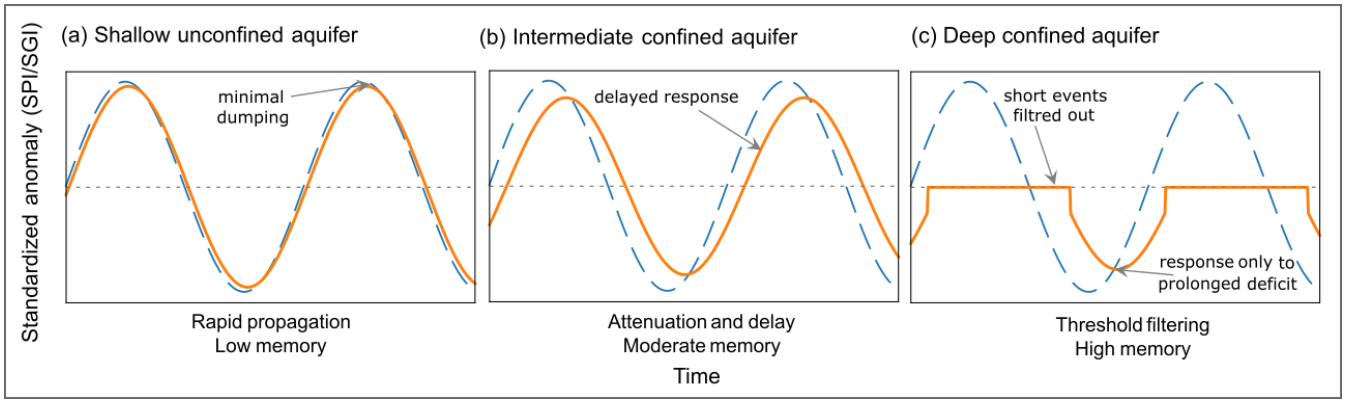

Figure 3: Conceptual model of groundwater drought propagation and recovery across aquifer systems. Schematic representation of SPI–SGI response behavior across groundwater systems of increasing depth and memory. Dashed lines indicate meteorological forcing (SPI), whereas solid lines represent groundwater response (SGI): (a) rapid propagation in the shallow unconfined aquifer, (b) attenuated and delayed response in the intermediate confined aquifer, and (c) threshold-like response in the deep confined aquifer.

4.1 Standardized Precipitation Index (SPI)

The Standardized Precipitation Index (SPI) was used to quantify meteorological drought at multiple time scales. SPI expresses the deviation of precipitation from the long-term climatology in units of standard deviation, allowing comparison between stations and regions with different climates (McKee et al., 1993; Guttman 1999; WMO, 2012).

Monthly precipitation totals from the five IMGW-PIB stations were first aggregated to 3-, 6-, and 12-month moving sums to represent short-term, seasonal, and annual-scale water balance conditions, respectively. The cumulative distribution function G(Pk) was then transformed to the standard normal distribution:

$$SPI = \Phi^{-1}\big(G(P_k)\big), \quad (1)$$

https://doi.org/10.5194/egusphere-2026-1904
Preprint. Discussion started: 10 June 2026

where Φ^{-1} is the inverse standard normal cumulative distribution function

Drought conditions were defined using commonly applied SPI thresholds (McKee et al., 1993; WMO, 2012). In this study, we adopt:

SPI < −1.0 moderate drought,

SPI < −1.5 severe drought,

SPI < −2.0 extreme drought.

For each time scale, drought events were identified as continuous periods during which SPI remained below a given threshold. For every event, we computed the duration (number of months), the minimum SPI value, and the accumulated severity (sum of SPI values below the threshold). These metrics were later compared with groundwater drought characteristics derived from SGI.

4.2 Standardized Groundwater Level Index (SGI)

The standardized groundwater index (SGI) was used to characterize groundwater drought conditions. SGI was calculated by standardizing groundwater level time series using a normal score transformation, as described by Bloomfield and Marchant (2013).

$$SGI_t = \Phi^{-1}(F(h_t)), \quad (2)$$

where: $F(h_t)$ is the cumulative distribution function of monthly groundwater levels, and Φ^{-1} is the inverse standard normal cumulative distribution function.

Drought conditions were defined as SGI < −1, with severity classes analogous to those used for SPI (Hisdal et al., 2001; Tallaksen & Van Lanen, 2004).

Both SPI and SGI were analyzed at consistent temporal scales to enable direct comparison of meteorological and groundwater drought dynamics (aggregation periods of 3, 6, and 12 months). Continuous periods below a given threshold were identified as drought events and summarised using standard drought metrics (see Section 4.3).

For aquifer-level analyses, individual SGI time series were grouped by aquifer level (unconfined, intermediate, or deep). Aquifer level means of SGI were computed by averaging SGI values across all wells belonging to the same level for corresponding months. Aquifer-level SGI series were used to derive drought metrics representative of each aquifer level. Part of the raw groundwater-level and meteorological time series used in this study had previously been compiled within an earlier MSc-level assessment of groundwater drought in GWB 43 (Jurzyk, 2025). However, in the present study, all input data were reprocessed within a substantially revised analytical framework, including a new expert-based piezometer classification, expanded event-based drought metrics, and the development of the Drought Impact and Pressure Index (DIPI). The methodological steps applied to derive these drought-response metrics and the final index are described in the following section.

https://doi.org/10.5194/egusphere-2026-1904
Preprint. Discussion started: 10 June 2026

4.3 Drought metrics

Based on the reprocessed monthly SGI-12 time series and the updated piezometer grouping, a set of event-based drought metrics was calculated to quantify groundwater system response, including vulnerability, maximum drought duration, resistance, resilience, propagation probability, and median recovery time. Drought events were defined as continuous periods with SGI < −1.0, and a set of metrics describing duration, severity, propagation and recovery was derived following established approaches (Van Loon, 2015; Peters et al., 2003; Thomas & Famiglietti, 2017).

The full set of applied drought metrics, together with their definitions and calculation formulas, is summarised in Table 2.

Table 2: Definitions and formulas of event-based groundwater drought metrics derived from SGI.

Metric	Symbol	Definition	Formula
Number of drought events	N	Total number of independent drought events (SGI < −1).	$N = J$
Duration	D	Length of a drought event in months.	$D_j = t_{end,j} - t_{start,j} + 1$
Severity	S	Cumulative SGI deficit during an event.	$S_j = \sum_{t \epsilon J_j} SGI_t$
Mean severity	S_{mean}	Average severity across all events.	$S_{mean} = \frac{1}{J} \sum_{j=1}^{J} S_j$
Mean intensity	I	Mean SGI value during drought events.	$I_j = \frac{1}{D_j} \sum_{t \epsilon J_j} SGI_t$
Minimum SGI	SGI_{min}	The most negative SGI value in the time series.	$SGI_{min} = \min(SGI_t)$
Resistance	CRT	Ability to avoid entering drought conditions.	$CRT = 1 - \frac{\sum_{t=1}^{T} D_t}{\sum_{=t=0}^{T} Z_t}$
Resilience	CRS	Probability of recovery from drought.	$CRS = \frac{\sum_t W_t}{T - \sum_t Z_t}$
Vulnerability	VUL	Maximum cumulative deficit across events.	$\mathrm{VUL} = \max_j \sum_{t \epsilon J_j} \lvert \mathrm{SGI_t} \rvert$
Propagation probability	P	Probability that short-term groundwater drought propagates into long-term groundwater drought.	$P = \frac{N_{SGI3 \rightarrow SGI12}}{N_{SGI3}}$
Propagation lag	L	Most frequent delay between SPI and SGI drought onset.	$L = mode(t^{SGI}_{start,j} - t^{SPI}_{start,j})$
Recovery time	R	Time required to return to near-normal conditions (SGI ≥ −0.5).	$R_j = t_{rec,j} - t_{min,j}$

SGI_t – Standardized Groundwater Level Index (SGI) at time t; t – time step (month); J – total number of drought events; J_j – set of time steps belonging to drought event j; $t_{start,j}$ and $t_{end,j}$ – start and end of event j; $t_{min,j}$ – time of minimum SGI within event j; $t^{SPI}_{start,j}$ – start time of the

https://doi.org/10.5194/egusphere-2026-1904
Preprint. Discussion started: 10 June 2026

corresponding meteorological drought event; $t_{rec,j}$ – the first time step after the event minimum when SGI ≥−0.5; D_t = 1 if SGI < 0, otherwise 0; Z_t = 1 if SGI ≥ 0, otherwise 0; W_t = 1 if transition from drought to non-drought occurs; T – total number of time steps; N_{SGI3} – number of short-term (SGI-3) groundwater drought events; $N_{SGI3 \rightarrow SGI12}$ – number of SGI-3 drought events that develop into SGI-12 drought events. The selected metrics collectively describe both the temporal characteristics of drought events and the dynamic response of groundwater systems, forming the basis for the exposure component of the Drought Impact Potential Index (DIPI) framework. All statistical analyses, SGI-based drought metrics, and figure generation were performed in Python within the Google Colab environment using custom scripts.

4.4 Lagged SPI–SGI correlation analysis

To examine how meteorological drought spreads into groundwater, we studied the relationships between the Standardized Precipitation Index (SPI) and the Standardized Groundwater Index (SGI) across multiple aggregation periods (3, 6, and 12 months), explicitly accounting for delayed groundwater response (Bloomfield & Marchant, 2013; Barker et al., 2016). For each groundwater cluster, SPI data was taken from the nearest precipitation station, based on geographic proximity to the cluster centroid. This approach preserves local precipitation variability relevant for recharge, while spatially averaged precipitation can conceal drought timing and severity (Shukla & Wood, 2008; Vicente-Serrano et al., 2010).

For each station–well pair, Pearson correlation coefficients were calculated between SPIk and SGI:

$$r = corr\left(SPI_k(t), SGI(t)\right) \quad (3)$$

where k = 3, 6, and 12 months.

For each aggregation scale, Pearson correlation coefficients were computed between SPIk(t) and SGI(t), and then extended to lagged correlations by shifting SGI relative to SPI over lags L=0–12 months:

$$r(L) = corr(SPI_k(t), SGI\ (t + L)) \quad (4)$$

where k = 3, 6, and 12 months.

The optimal lag for each cluster and scale was identified as the lag with the highest absolute correlation, indicating the main delay involved in recharge, storage, and transit processes (Bloomfield & Marchant, 2013; Barker et al., 2016; Chen et al., 2024). To evaluate robustness against co-trending, analyses were repeated on detrended indices; interpretation depended on observing consistent patterns in both versions. A complete matrix of SPI–SGI correlations across different aggregation scales is available in Appendix B.

4.5 Spatial analysis and Drought Impact Potential Index (DIPI)

This section represents the core methodological contribution of the study. To assess the spatial distribution of drought impact potential within GWB 43, we developed a composite Drought Impact Potential Index (DIPI) integrating exposure to groundwater drought, anthropogenic pressure, and system sensitivity. This approach is inspired by multidimensional

https://doi.org/10.5194/egusphere-2026-1904
Preprint. Discussion started: 10 June 2026

vulnerability indices in water resources and drought risk assessments (e.g., Tallaksen & Van Lanen, 2004; Van Loon et al., 2016), and is adapted here to hydrogeological conditions.

Point attributes from monitoring piezometers (cluster ID, SGI-12 drought metrics) serve as primary spatial anchors. Continuous surface representations of drought performance (e.g., Vulnerability, Resilience) were generated through spatial interpolation (e.g., Inverse Distance Weighting, kriging) to enable comparison with other spatial drivers. Interpolation was constrained within the GWB 43 boundary to prevent artifacts outside the study area (e.g., Goovaerts, 1997; Hengl, 2009).

We focus on metrics derived from the 12-month Standardized Groundwater Index (SGI-12) because multi-year aggregations better reflect long-term groundwater drought persistence and have stronger relationships with hydrological impacts compared to shorter windows (Bloomfield & Marchant, 2013; Kumar et al., 2016).

The Drought Impact Potential Index (DIPI) is defined as a weighted sum of three components: Exposure (E), Pressure (P), and Sensitivity (S). Weights indicate the relative influence of climatic/hydrological forcing (E) and human/environmental conditions (P, S) on drought impacts, following methods in compound risk assessment (e.g., Wheater & Evans, 2009; Porter et al., 2014).

All components and sub-components were normalized using min–max scaling prior to aggregation, as shown in Table 3.

Table 3: Components, sub-components, and aggregation equations of the Drought Impact Potential Index (DIPI).

Component	Sub-component	Symbol	Definition	Formula
Exposure (E)	Vulnerability	VUL′	Maximum cumulative groundwater deficit	$VUL' = \frac{VUL - VUL_{min}}{VUL_{max} - VUL_{min}}$
Exposure (E)	Inverse resilience	CRS_{inv}'	Inverted resilience	$CRS_{inv}' = 1 - \frac{CRS - CRS_{min}}{CRS_{max} - CRS_{min}}$
Exposure (E)	Maximum duration	MaxDur′	Maximum duration of drought events	$MaxDur' = \frac{MaxDur - MaxDur_{min}}{MaxDur_{max} - MaxDur_{min}}$
Exposure (E)	Composite exposure	E	Combined drought severity and persistence	$E = 0.4VUL' + 0.3CRS_{inv}' + 0.3MaxDUR'$
Pressure (P)	Abstraction density	Q_{dens}'	Groundwater abstraction density	$Q_{dens}' = \frac{Q_{dens} - Q_{dens_{min}}}{Q_{dens_{max}} - Q_{dens_{min}}}$
Pressure (P)	Mining impact	Mining′	Mining-induced groundwater drawdown intensity	—
Pressure (P)	Composite pressure	P	Anthropogenic stress	$P = 0.7Q_{dens}' + 0.3Mining'$
Sensitivity (S)	GDE	GDE′	Groundwater dependent ecosystems	—
Sensitivity (S)	Quality	Quality′	Groundwater quality	—

https://doi.org/10.5194/egusphere-2026-1904
Preprint. Discussion started: 10 June 2026

Sensitivity (S)	Composite sensitivity	S	Environmental vulnerability	$S = 0.5GDE' + 0.5Qaulity'$
Drought Impact Potential Index		DIPI	Integrated drought impact index	$DIPI = 0.4E + 0.3P + 0.3S$

Variables marked with (′) denote normalized values (0–1) obtained using min–max scaling; CRS_{inv}' – inverted and normalized resilience (1−CRS); — Mining′, GDE′, and Quality′ are spatially derived indicators normalized to the range 0–1. All composite indices are dimensionless. All sub-components are first normalized to the interval [0, 1] to ensure comparability. For variables where higher values indicate lower risk (e.g., resistance/resilience), normalization is inverted, as shown above. The composite DIPI combines the components with the predefined weights.

Final DIPI values are mapped using continuous surfaces (interpolated from piezometer measurements) and classified into quantiles for cartographic visualization. The full spatial representation of all normalized sub-components and both DIPI aggregation schemes is provided in Appendix A (Fig. A1) to ensure methodological transparency and reproducibility of the framework. All intermediate datasets, reproducible notebooks, and figure source tables are openly archived in Zenodo (Sawicka and Jurzyk, 2026).

To further disentangle the relative contributions of exposure and pressure, a spatial contrast index was computed as the difference between normalized exposure and pressure components (E − P). This metric highlights areas dominated by exposure-driven processes versus those controlled by anthropogenic pressure.

5. Results

5.1 Standardized Precipitation Index (SPI)

The temporal evolution of the SPI calculated for 3-, 6-, and 12-month aggregation windows reveals a largely coherent drought signal across the five precipitation stations. Although individual stations show some differences in amplitude, most drought episodes occur synchronously, indicating regionally consistent atmospheric forcing.

For SPI-3, several short and intense droughts are evident, with minima below −3 at most stations. At the 6-month scale, droughts become less abrupt but more persistent, with the most significant regional event centered in 2003, when the areal mean dropped to −2.93. The 12-month SPI emphasizes the multi-year nature of this episode, with the lowest areal value of −2.69 recorded in late 2003.

Overall, the mean SPI closely tracks individual stations, confirming that major drought episodes were spatially widespread rather than localized.

https://doi.org/10.5194/egusphere-2026-1904
Preprint. Discussion started: 10 June 2026

5.2 Standardized Groundwater Level Index (SGI)

The SGI calculated for 3-, 6-, and 12-month aggregation windows reveals marked spatial differences between groundwater clusters. Although all clusters experienced periods of negative SGI, the timing and magnitude of the minima vary.

For SGI-3, the most severe groundwater droughts happened in Cluster 2 in late 2021 (minimum −2.63) and in Cluster 3 in late 2023 (minimum −2.40). Cluster 1 experienced a shorter but clear event around 2014 (minimum −1.98). At the 6-month scale, droughts appear smoother and last longer, with Cluster 3 showing the deepest anomaly (−2.40), followed by Cluster 2 (−1.97). SGI-12 shows a long-lasting depletion signal in Cluster 3 that stays below −2.3 into 2024 (minimum −2.39), while Clusters 1 and 2 have shallower, long-term deficits (−1.52 and −1.51, respectively).

Overall, the strongest and most persistent groundwater drought signal is consistently expressed in Cluster 3 across all aggregation windows, whereas Clusters 1 and 2 exhibit shorter or less severe episodes (Fig.4).

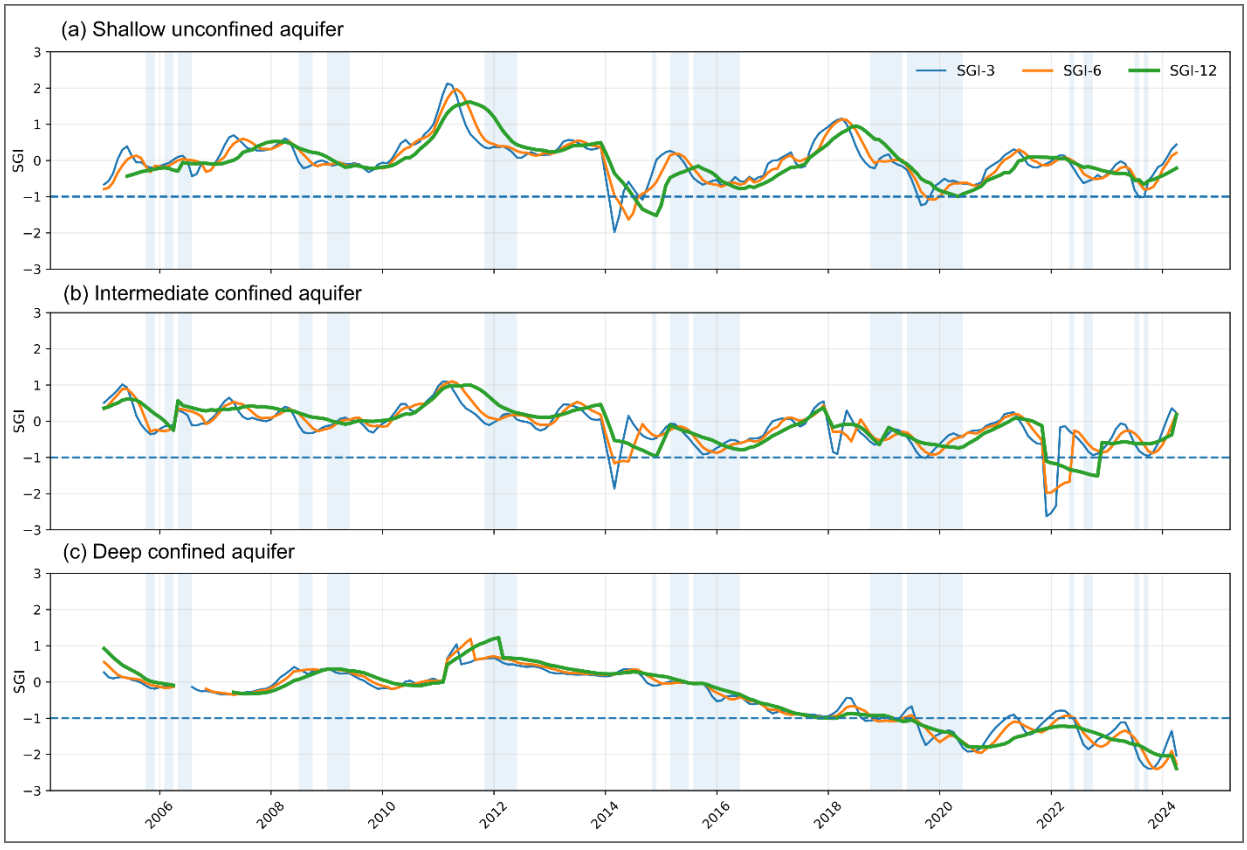

Figure 4: Temporal changes in SGI across aquifer systems and aggregation levels in GWB 43. Cluster-mean SGI-3, SGI-6, and SGI-12 time series for the three groundwater systems in GWB 43: (a) shallow unconfined, (b) intermediate confined, and (c) deep confined aquifer. The dashed horizontal line indicates the groundwater drought threshold (SGI = −1). Shaded areas show periods of meteorological drought used for comparing with groundwater response timing and duration.

https://doi.org/10.5194/egusphere-2026-1904
Preprint. Discussion started: 10 June 2026

To ensure comparability across aquifer systems, time series were truncated to the common observation period (2005–2024). As shown in Appendix B (Fig. B1), the full lagged Pearson correlation matrices confirm the strongest and fastest SPI–SGI coupling in the shallow unconfined aquifer, whereas the confined systems display weaker and delayed responses.

5.3 Drought metrics

Groundwater drought characteristics derived from SGI reveal distinct differences between clusters and scales of aggregation (Tab. 4; Fig. 5). At SGI-3, droughts tend to be frequent but short. Cluster 1 experienced four events with an average duration of 2 months and a maximum of 3 months, while Cluster 2 shows greater severity (−3.93). Cluster 3 has longer events, averaging 11 months with a maximum of 23 months, and a mean severity of −17.07.

At SGI-6, events become fewer and longer. Cluster 2 experienced four events (average of 4 months; maximum of 6 months), while Cluster 1 had shorter events. Cluster 3 shows longer and more persistent droughts.

At SGI-12, droughts are primarily characterized by multi-year events. Cluster 3 features two events lasting over 50 months with the highest severity (−45.83). Clusters 1 and 2 experience shorter, less severe droughts.

Table 4: Groundwater drought metrics across aquifer systems and SGI aggregation scales in GWB 43. Abbreviations: VUL – vulnerability; CRT – resistance; CRS – resilience.

SGI	Cluster	N	Mean dur.	Max dur.	Mean sev.	Prop.	Recovery	CRT	CRS	VUL
SGI-3	1	4	2	3	-2.6	0.25	7	0.90	0.09	12.7
SGI-3	2	2	3	5	-4.4	0.14	11	0.90	0.11	22.2
SGI-3	3	1	6	6	-8.2	0.17	32	0.95	0.05	118.1
SGI-6	1	5	2	3	-3.9	0.31	10	0.91	0.09	13.5
SGI-6	2	4	4	6	-5.6	0.44	17	0.94	0.07	24.3
SGI-6	3	2	7	12	-9.2	0.07	31	0.97	0.03	122.6
SGI-12	1	5	11	23	-17.1	0.40	n.r.	0.96	0.03	25.3
SGI-12	2	3	20	31	-30.5	0.47	n.r.	0.96	0.06	25.2
SGI-12	3	2	31	61	-47.0	0.48	n.r.	0.98	0.03	122.4

n.r. – no recovery observed within the observation period.

Resilience decreases as SGI aggregation windows lengthen, while resistance rises. Cluster 3 shows consistently high vulnerability across all SGI scales, with low resilience. Resistance increases with longer SGI aggregation, indicating the cumulative buffering capacity of groundwater systems. Median recovery also grows with aggregation scale and reaches 'no recovery' (n.r.) at SGI-12 for all clusters (Fig.5c).

https://doi.org/10.5194/egusphere-2026-1904
Preprint. Discussion started: 10 June 2026

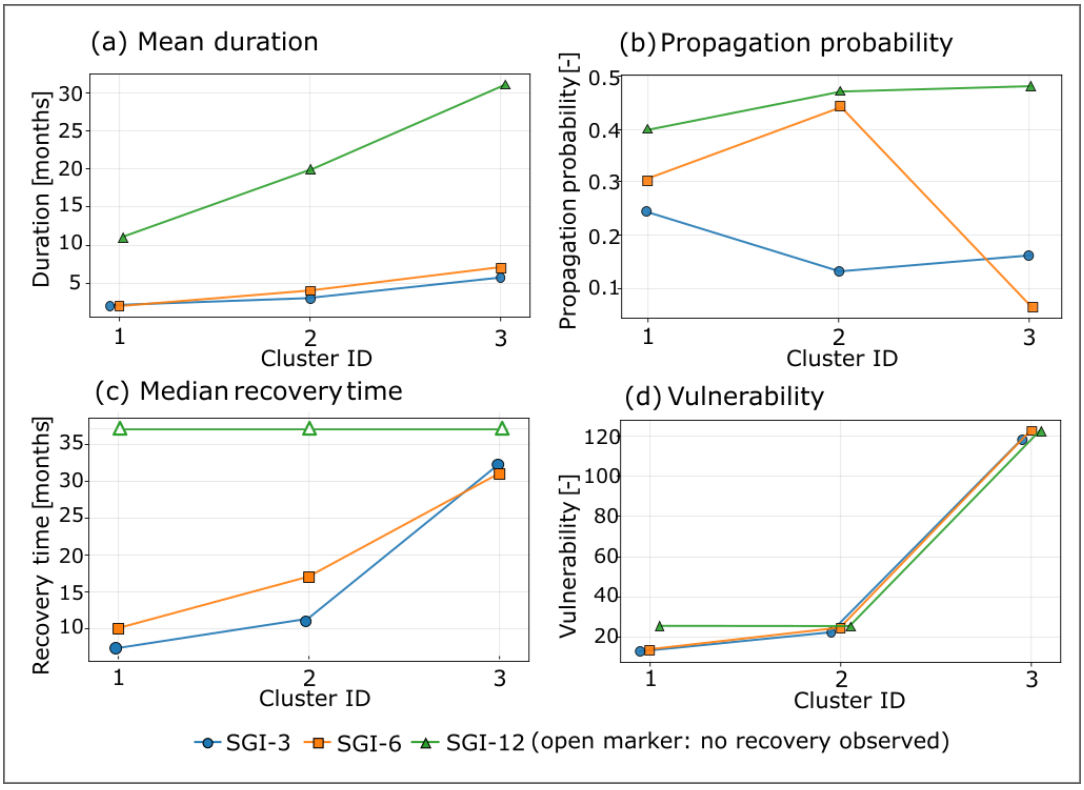

315 **Figure 5:** Groundwater drought metrics across aquifer systems and timescales. Comparison of drought metrics derived from SGI-3, SGI-6, and SGI-12 for the three aquifer systems in GWB 43: (a) mean drought duration, (b) propagation likelihood, (c) median recovery time, and (d) vulnerability (VUL). Open markers in panel (c) indicate cases where recovery to near-normal conditions (SGI ≥ −0.5) was not observed within the study period.

Figure 5 shows systematic differences in drought patterns across groundwater systems. Duration and vulnerability rise sharply
320 with system depth, while propagation probability follows non-linear trends, especially in the deep confined system. Recovery time increases with aggregation scale and becomes nearly unbounded at SGI-12, indicating ongoing drought conditions.

5.4. Groundwater drought propagation and recovery dynamics

Propagation probability increases with aggregation scale. At short timescales (SGI-3), propagation remains limited across all clusters, whereas at longer timescales (SGI-12) it becomes substantial, particularly in Clusters 2 and 3 (Fig.6).

325 Clear differences appear among the clusters. Cluster 1 shows low propagation probability and quick response, suggesting a system closely linked to short-term recharge. Cluster 2 demonstrates intermediate behavior, where propagation only becomes significant at seasonal to annual scales. Meanwhile, Cluster 3 exhibits delayed but ultimately strong propagation, matching a system with long memory and cumulative storage effects.

https://doi.org/10.5194/egusphere-2026-1904
Preprint. Discussion started: 10 June 2026

Recovery times increase substantially with the aggregation scale and differ substantially across clusters. Cluster 1 recovers rapidly after drought events, typically within a few months, indicating high system resilience. Cluster 2 exhibits delayed recovery, suggesting partial storage depletion during consecutive dry periods. In Cluster 3, recovery is extremely limited, with groundwater levels often failing to return to near-normal conditions within the observation period.

These dynamics are reflected in the performance metrics: increasing resistance (CRT) and decreasing resilience (CRS) with longer aggregation scales, together with high vulnerability (VUL) in Cluster 3, confirm that groundwater systems become progressively less capable of recovering from prolonged deficits.

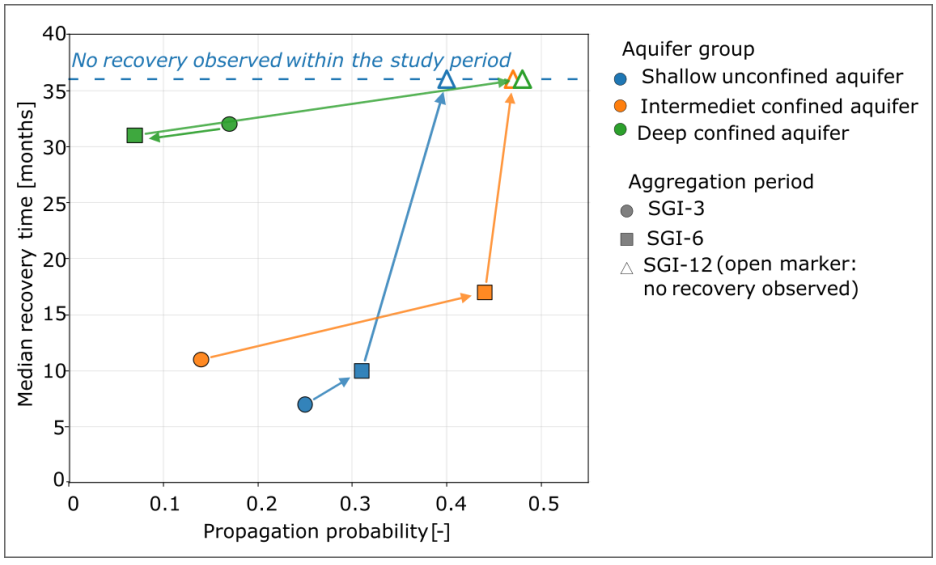

Figure 6: Groundwater drought propagation–recovery trajectories across aquifer systems. Shows the relationship between groundwater drought propagation probability and median recovery time for shallow, intermediate, and deep aquifers in GWB 43. Marker shape indicates the temporal aggregation scale (SGI-3, SGI-6, SGI-12), while arrows depict the system's response trajectory as temporal integration increases. Open markers at the upper reference line signify no observed recovery within the common observation period.

Figure 6 highlights contrasting propagation–recovery behavior among aquifer systems. In the shallow and intermediate systems, the probability of propagation increases with aggregation scale, along with longer recovery times. In contrast, the deep confined system shows non-monotonic behavior, with a decrease in propagation from SGI-3 to SGI-6, followed by an increase at SGI-12. This reflects temporal filtering of short-term deficits and a threshold-type response to prolonged forcing.

In the deep confined system, propagation probability decreases from SGI-3 to SGI-6, indicating that short-term groundwater anomalies do not translate into sustained seasonal-scale drought. This reflects temporal filtering of recharge deficits and suggests a minimum duration threshold for drought propagation in the deep aquifer.

https://doi.org/10.5194/egusphere-2026-1904
Preprint. Discussion started: 10 June 2026

5.5. Drought Impact Potential Index (DIPI)

To evaluate the sensitivity of the DIPI formulation to the weighting scheme, both a weighted (0.4E + 0.3P + 0.3S) and an unweighted (E + P + S)/3 approach were applied. The strong spatial agreement between the equal-weight and weighted DIPI variants (Appendix A, Fig. A1 f, i) confirms that the identified hotspot configuration is robust to the aggregation scheme.

The resulting maps exhibit a highly consistent spatial pattern, with the main high-index zones preserved in both cases. In particular, a coherent high-DIPI area is observed in the central and southern parts of the groundwater body, whereas lower values predominate in the northern sector (Fig. 7).

Differences between the two formulations are limited to minor variations in class boundaries and local intensity, without affecting the overall spatial configuration of hotspots. This indicates that the DIPI pattern is robust with respect to the assumed weighting scheme. The spatial configuration of high- and low-value areas remains largely unchanged between panels, indicating a stable distribution of index values. Variations between panels are limited to minor changes in intensity and class boundaries.

https://doi.org/10.5194/egusphere-2026-1904
Preprint. Discussion started: 10 June 2026

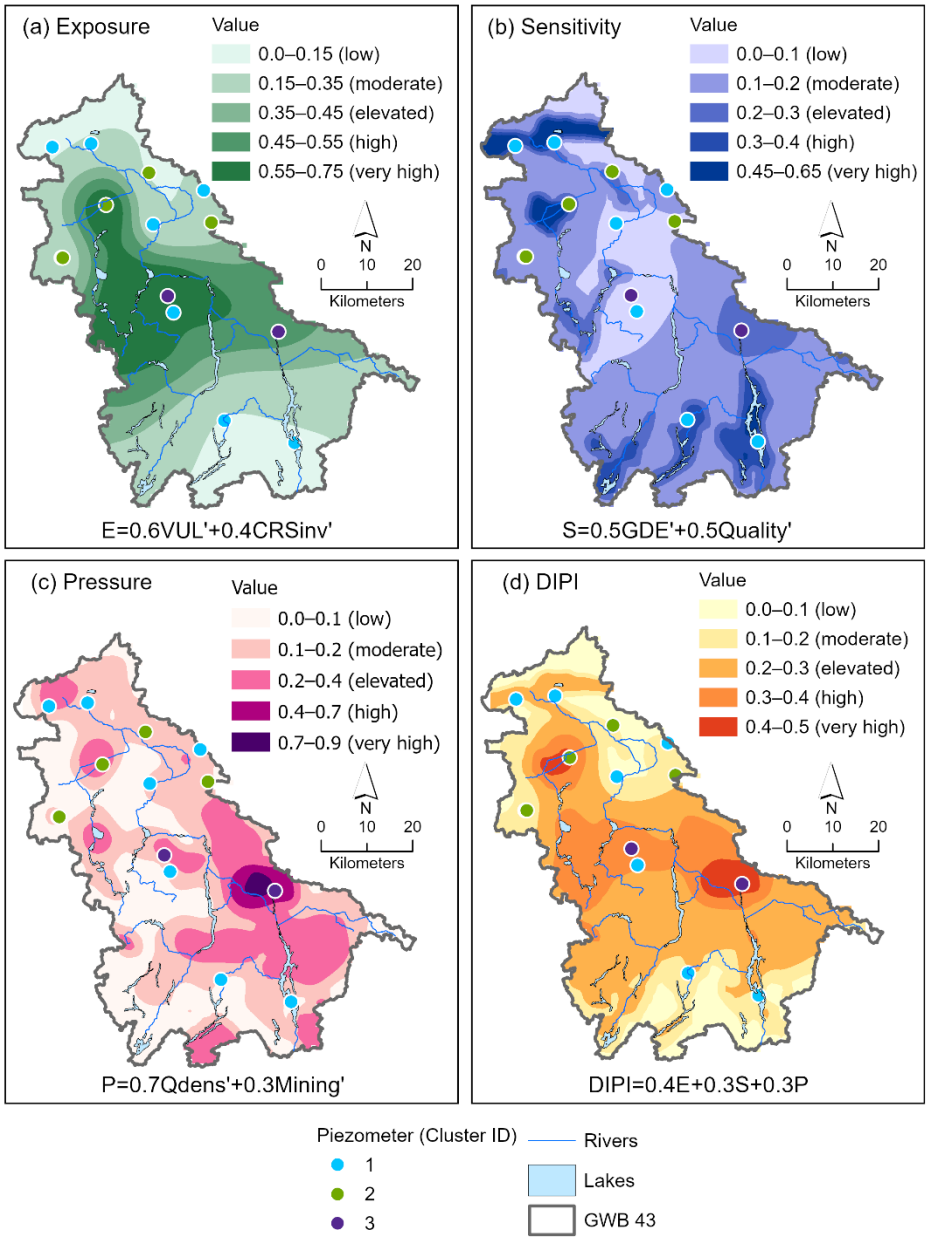

360

Figure 7: Spatial distribution of DIPI and its component layers in GWB 43. Spatial distribution of the Drought Impact Potential Index (DIPI) and its component layers: (a) Exposure (E), (b) Sensitivity (S), (c) Pressure (P), and (d) final DIPI. Exposure integrates process-based groundwater drought metrics, sensitivity reflects GDE and groundwater-quality constraints, and pressure represents abstraction density and mining-related stress. All components were normalized to the 0–1 range prior to
365 integration.

https://doi.org/10.5194/egusphere-2026-1904
Preprint. Discussion started: 10 June 2026

Aggregation of DIPI at the cluster level showed a clear increase from shallow unconfined aquifers (0.195) to intermediate confined systems (0.219), with the highest average value found in deep confined aquifers (0.407). This pattern suggests that the increased drought impact potential in deeper aquifer systems is mainly driven by greater exposure rather than significant differences in sensitivity.

5.6. Exposure–pressure contrast

The spatial contrast between normalized exposure (E) and pressure (P) components within GWB 43, expressed as E – P, shows mostly positive values across the study area, with some localized zones of negative values. Positive values suggest areas where drought impact potential is mainly driven by the natural groundwater system response, while negative values indicate zones dominated by human activities. Near-zero values represent balanced conditions where both components contribute equally (Fig. 8). The map shows that most areas are exposure-driven, with pressure-dominated zones limited to small patches. Area-based classification of the exposure–pressure contrast (E − P) reveals that exposure-dominated zones make up 60.4% of GWB 43, pressure-dominated areas account for 21.8%, and balanced conditions, where both components are similar, cover 17.8% of the study area.

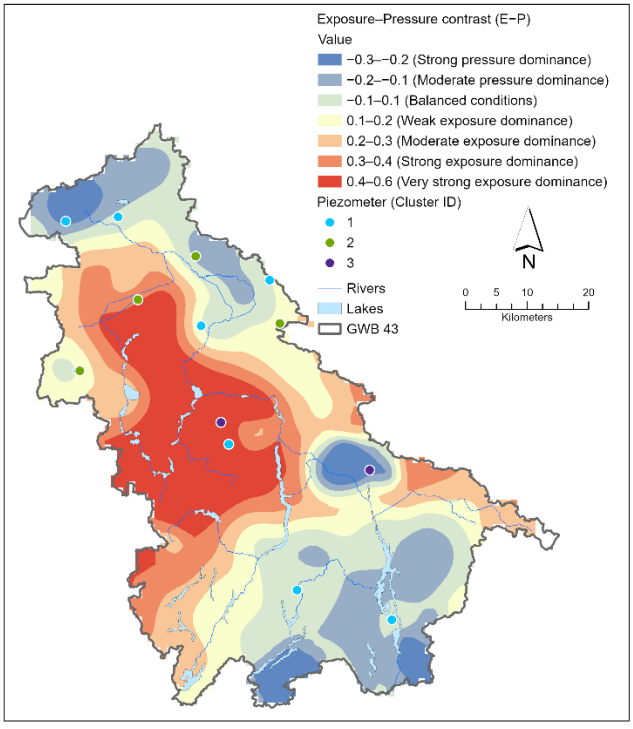

Figure 8: Exposure–pressure contrast map of groundwater drought controls in GWB 43.

https://doi.org/10.5194/egusphere-2026-1904
Preprint. Discussion started: 10 June 2026

Spatial contrast between normalized Exposure (E) and Pressure (P) is expressed as E − P. Positive values indicate areas dominated by the natural aquifer-system response, while negative values highlight zones where human activity has a greater influence on groundwater drought impact. Values close to zero suggest a balanced effect of both factors.

6. Discussion

The combined analysis of time series, propagation–recovery relationships, and aggregated drought metrics reveals a clear system-dependent control on groundwater drought behavior in GWB 43. Shallow unconfined systems respond rapidly to meteorological forcing, with high propagation efficiency and relatively fast recovery, reflecting limited storage and low system memory. In contrast, intermediate systems exhibit attenuated and delayed responses, indicating partial decoupling from short-term recharge variability. The deep confined system shows fundamentally different dynamics, characterized by non-linear propagation, threshold-type response, and extremely long or absent recovery.

These results integrate groundwater drought into a process-based framework, where the system response is driven by the interaction between external forces and internal aquifer characteristics, consistent with recent large-sample groundwater studies (Ebeling et al., 2025).

6.1 System memory and aquifer depth

The results show that groundwater drought behavior is strongly influenced by system memory, which systematically varies with aquifer depth and hydrogeological structure. Shallow systems respond quickly to short-term changes in recharge, experiencing frequent but temporary drought episodes. Conversely, deeper systems have delayed responses, longer drought durations, and persistent water deficits, reflecting the cumulative effect of recharge over extended periods.

This behavior aligns with previous research emphasizing the importance of aquifer storage and hydraulic connectivity in regulating groundwater memory (Van Loon, 2015; Bloomfield & Marchant, 2013). Recent studies further verify that groundwater response times and memory are heavily influenced by aquifer depth and hydrogeological conditions (Ebeling et al., 2025).

Furthermore, recent studies of the land water cycle show that hydrological memory greatly increases from atmospheric to underground parts, with groundwater showing the strongest persistence and long-term storage effects (Berghuijs et al., 2025). As a result, deeper and more confined systems display smoother but more persistent drought signals, while shallow systems maintain closer connection with atmospheric forcing. These findings confirm that groundwater drought cannot be viewed simply as a reaction to precipitation anomalies, but must be understood as influenced by aquifer structure and internal system dynamics.

6.2 Propagation and recovery asymmetry

https://doi.org/10.5194/egusphere-2026-1904
Preprint. Discussion started: 10 June 2026

A key finding of this study is the clear imbalance between drought propagation and recovery processes. While propagation happens when meteorological deficits build up enough to decrease recharge, recovery depends on sustained and often extended recharge input, making it inherently slower and more limited.

This asymmetry is especially clear in deeper systems, where droughts happen less often but, once they start, last longer and recover slowly. In contrast, shallow systems show both quick spread and quick recovery, reflecting a more active but less lasting response pattern.

Recent studies increasingly emphasize that drought propagation and recovery are governed by fundamentally different mechanisms: propagation by cumulative deficits and recovery by recharge conditions and storage dynamics (Van Loon et al., 2016; Barker et al., 2016; Jasechko, 2026).

This decoupling explains why groundwater drought persists even after meteorological conditions improve and points out the limitations of interpreting groundwater drought only through climatic indices.

The substantial share of pressure-dominated areas (21.8%) indicates that anthropogenic forcing exerts a spatially significant control on groundwater drought impact in GWB 43, yet the predominance of exposure-driven zones confirms that intrinsic system properties remain the primary factor governing drought persistence and spatial variability.

Notably, pressure-dominated zones mainly align with areas affected by mining-related dewatering, indicating that human-induced drawdown locally intensifies groundwater drought signals, while the larger spatial pattern remains driven by aquifer-scale storage and recovery processes.

6.3 Process-based interpretation of the DIPI framework

The cluster-level DIPI gradient supports the interpretation that aquifer architecture exerts a first-order control on drought impact potential. The substantially higher DIPI in deep confined systems suggests that prolonged event duration and larger cumulative severity outweigh their only moderately different sensitivity, leading to a markedly stronger integrated drought-risk signal. The stability of the DIPI spatial pattern across various weighting schemes shows that the index reflects inherent properties of the groundwater system rather than model configuration artifacts. The agreement between weighted and unweighted versions indicates that the relative roles of exposure, pressure, and sensitivity do not change the core spatial structure of drought impact potential.

Unlike traditional vulnerability indices that rely on static indicators or expert judgment, the exposure component specifically includes process-based drought metrics that connect spatial patterns to groundwater system dynamics. This method aligns with recent advances in drought research emphasizing dynamic system responses and process-based understanding of drought phenomena (Kumar et al., 2020; Vega Briones et al., 2024; Kartal & Nones, 2024).

DIPI reflects a synthesis of observed system responses rather than a purely statistical aggregation. Spatial patterns thus emerge from the interaction between external forcing and internal system properties, offering a physically grounded interpretation of groundwater drought vulnerability.

https://doi.org/10.5194/egusphere-2026-1904
Preprint. Discussion started: 10 June 2026

6.4 Anthropogenic pressure and mining effects

Anthropogenic pressure, especially mining-related dewatering, adds an extra influence on groundwater drought dynamics by altering hydraulic gradients and storage conditions. Long-term drainage from open-pit mining lowers groundwater levels and can intensify the impacts of meteorological deficits, effectively decreasing the threshold for drought initiation.

Recent studies increasingly distinguish between climate-driven and human-modified groundwater drought, highlighting that anthropogenic pressures may significantly alter natural system response and drought persistence (Vega Briones et al., 2024; Jasechko et al., 2026).

In such systems, the distinction between natural drought and anthropogenically induced drawdown becomes less clear, as both processes interact within the same hydraulic framework. This interaction may enhance drought persistence and delay recovery, especially in deeper or hydraulically connected aquifers.

The results show that mining-induced drawdown amplifies drought conditions locally, while the overall spatial pattern is governed by aquifer-scale processes.

6.5 Limitations and implications

Several limitations should be recognized. Spatial interpolation adds uncertainty due to data density and method choice. The use of SGI aggregation scales affects the depiction of drought persistence, and the pressure component relies on simplified indicators of abstraction and mining activity.

Despite these limitations, the integrated framework offers a consistent foundation for connecting groundwater drought dynamics with spatial vulnerability patterns and provides a process-oriented approach for evaluating groundwater drought under combined climatic and human influences.

7. Conclusions

This study demonstrates that groundwater drought vulnerability in GWB 43 arises from the interactions among climatic forcing, aquifer memory, anthropogenic pressure, and environmental sensitivity within a unified Drought Impact Potential Index (DIPI) framework. The results demonstrate that this objective has been successfully achieved.

The analysis reveals that groundwater drought behavior varies systematically across aquifer types. Shallow unconfined systems respond and recover quickly, while deeper confined systems show delayed effects, prolonged drought periods, and limited recovery. These variations are evident in drought metrics derived from SGI and suggest that aquifer storage and system memory are key factors influencing the persistence of groundwater droughts.

A key finding is the asymmetry between drought propagation and recovery. While spread is driven by the buildup of meteorological deficits, recovery needs ongoing recharge and is therefore significantly slower, particularly in deeper systems.

https://doi.org/10.5194/egusphere-2026-1904
Preprint. Discussion started: 10 June 2026

This results in extended groundwater drought even after meteorological conditions improve, as shown in the analyzed time series and recovery metrics.

The spatial analysis indicates that the impact of groundwater drought is mainly driven by inherent system properties. Exposure-dominated areas make up about 60% of the study area, while pressure-dominated zones (around 22%) are limited in size and mostly linked to mining-related dewatering. This indicates that human activities mainly serve as local boosters of drought, while the overall spatial pattern is controlled by aquifer-scale processes.

The proposed DIPI framework proved robust to weighting assumptions and effectively captures the interaction among system response, anthropogenic pressure, and environmental sensitivity. By incorporating process-based drought metrics into the exposure component, the approach provides a physically grounded link between groundwater drought dynamics and spatial vulnerability patterns, which is not explicitly represented in conventional static index-based approaches.

Although the pressure component relies on proxy indicators rather than direct measurements of abstraction rates and mining dewatering volumes, the consistent spatial patterns suggest that the identified relationships accurately reflect strong system-scale controls. Overall, the results demonstrate that groundwater drought in GWB 43 cannot be explained solely by climatic forcing but must be understood as the outcome of interactions among meteorological conditions, aquifer properties, and human pressures. The proposed framework provides a transferable approach for assessing groundwater drought vulnerability in complex hydrogeological systems and offers a basis for improved groundwater management amid increasing climatic and human stresses.

Appendix A

https://doi.org/10.5194/egusphere-2026-1904
Preprint. Discussion started: 10 June 2026

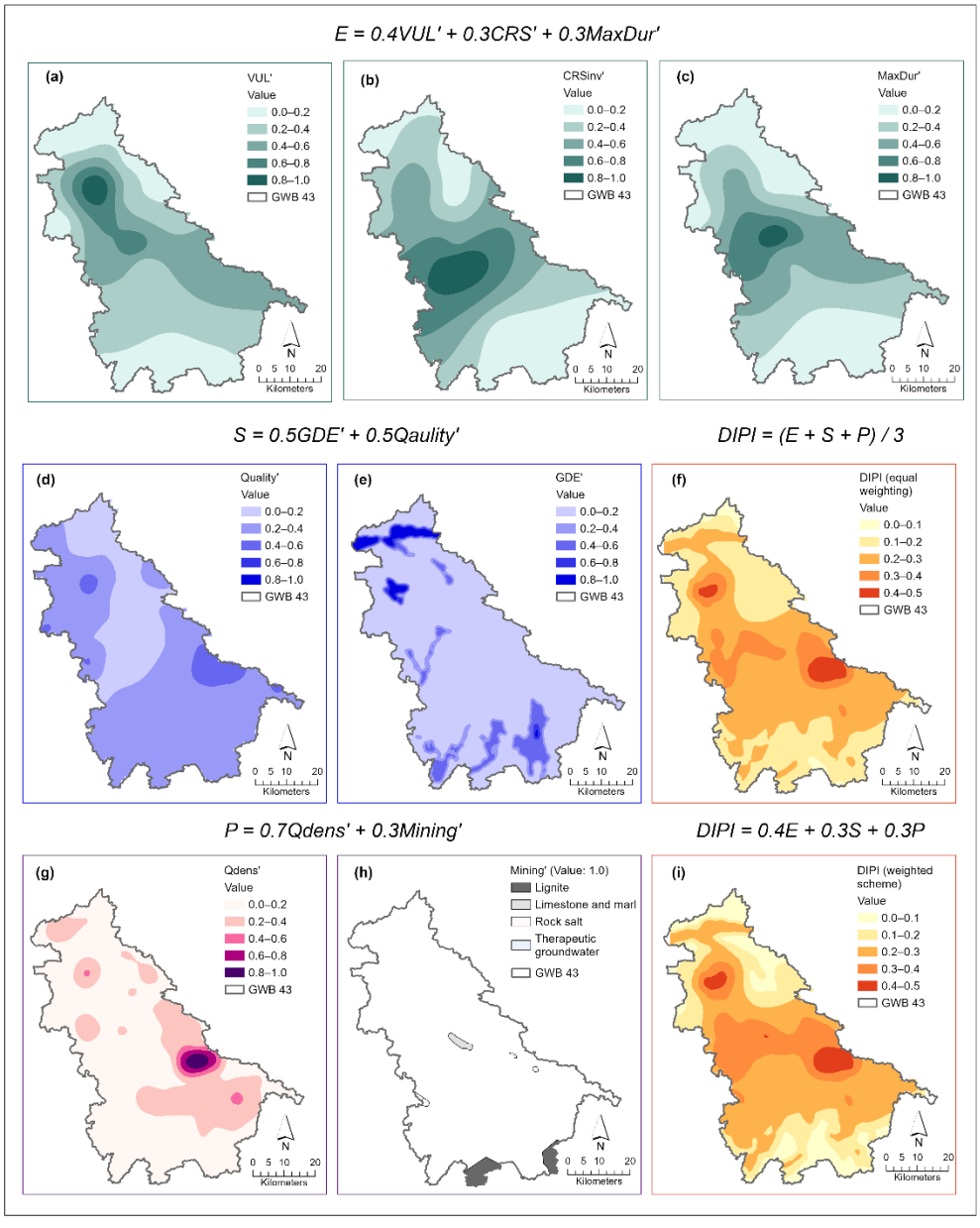

Figure A1: Spatial distribution of normalized DIPI sub-components and comparison of aggregation schemes. Panels (a–c) present the normalized exposure metrics (VUL′, CRSinv′, MaxDur′), panels (d–e) the sensitivity layers (Quality′, GDE′), and panels (g–h) the pressure layers (Qdens′, Mining′). Panels (f) and (i) compare the equally weighted and weighted DIPI variants, respectively, highlighting the spatial robustness of hotspot patterns.

https://doi.org/10.5194/egusphere-2026-1904
Preprint. Discussion started: 10 June 2026

Appendix B

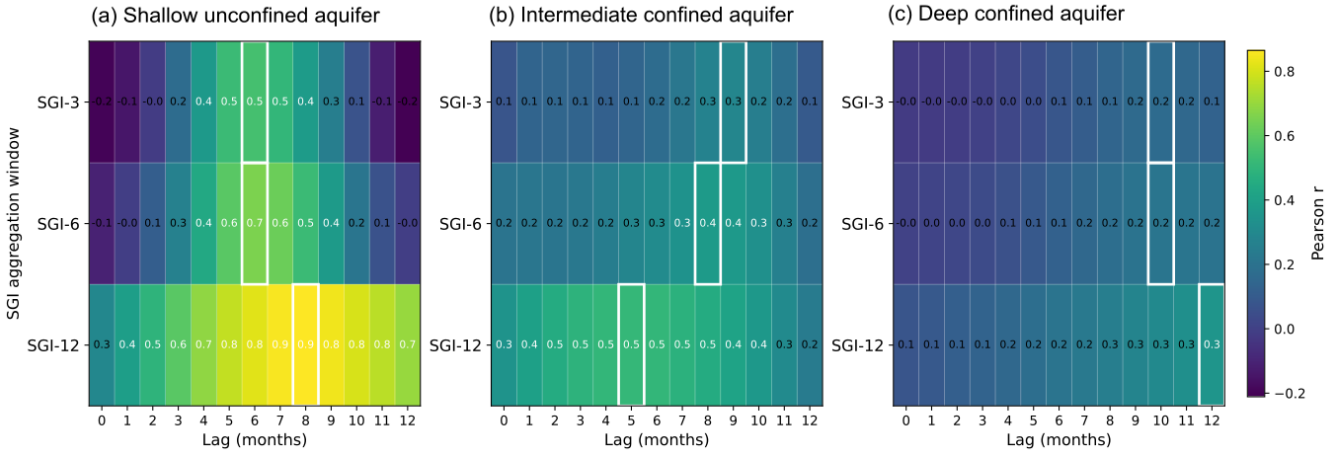

Figure B1: Lagged Pearson correlations between SPI and SGI for the three groundwater clusters: (a) shallow unconfined aquifer, (b) intermediate confined aquifer, and (c) deep confined aquifer. Rows represent SGI aggregation windows (3, 6, and 12 months), whereas columns represent SPI lags from 0 to 12 months based on the nearest precipitation station. The heatmaps reveal clear differences in drought propagation strength and response timing among clusters, with the shallow unconfined aquifer showing the strongest and fastest response.

Author contributions

KS designed the study concept and analytical framework, including the piezometer classification, drought-response metrics, and DIPI construction. KS performed the analyses, prepared all figures, interpreted the results, supervised the study, and wrote the manuscript. KJ compiled, curated, and quality-checked the original groundwater and meteorological datasets during the preceding MSc-level study and contributed to data validation in the present work. Both authors revised and approved the final manuscript.

Disclaimer

Copernicus Publications remains neutral with regard to jurisdictional claims made in the text, published maps, institutional affiliations, or any other geographical representation in this paper. While Copernicus Publications makes every effort to include appropriate place names, the final responsibility lies with the authors. Views expressed in the text are those of the authors and do not necessarily reflect the views of the publisher.

https://doi.org/10.5194/egusphere-2026-1904
Preprint. Discussion started: 10 June 2026

Acknowledgements

The authors acknowledge the Polish Geological Institute – National Research Institute (PIG-PIB) and the Polish Hydrogeological Survey for maintaining the national groundwater monitoring network and for providing access to the long-term piezometric records used in this study. Meteorological observations were provided by IMGW-PIB. Data processing and spatial analyses were supported by the GIS and computational facilities of the Faculty of Geology, University of Warsaw.

AI use statement

Generative AI tools (ChatGPT) were used exclusively for language refinement and stylistic editing of selected parts of the manuscript. All scientific interpretations, methodological decisions, calculations, and final text verification were performed by the authors.

Code and data availability

The minimal reproducible input datasets, processed analytical outputs, figure source data, reproducible Jupyter notebooks, and the master workflow description used in this study are openly available via GitHub and archived on Zenodo (Sawicka and Jurzyk, 2026; https://doi.org/10.5281/zenodo.19371351). The repository includes stepwise preprocessing, drought-metric, DIPI-construction, and figure-generation workflows, along with a master reproducibility entry point that describes the full analytical chain. Raw institutional groundwater monitoring data from the Polish Hydrogeological Survey (PIG-PIB) are subject to access restrictions and cannot be redistributed. To ensure full reproducibility, the repository provides the processed monthly monitoring series used as analytical inputs, together with all derived standardized drought indices, drought metrics, DIPI components, and figure source tables used directly in the analyses.

Competing interests

The authors declare that they have no conflict of interest.

Financial support

This research received no specific grant from any funding agency in the public, commercial, or not-for-profit sectors.

References

Barker, L. J., Hannaford, J., Chiverton, A., and Svensson, C.: From meteorological to hydrological drought using standardised indicators, Hydrol. Earth Syst. Sci., 20, 2483–2505, https://doi.org/10.5194/hess-20-2483-2016, 2016.

https://doi.org/10.5194/egusphere-2026-1904
Preprint. Discussion started: 10 June 2026

Berghuijs, W. R., Woods, R. A., and Hrachowitz, M.: Annual memory in the terrestrial water cycle, Hydrol. Earth Syst. Sci., 29, 1319–1335, https://doi.org/10.5194/hess-29-1319-2025, 2025.

Bloomfield, J. P., and Marchant, B. P.: Analysis of groundwater drought building on the standardised precipitation index approach, Hydrol. Earth Syst. Sci., 17, 4769–4787, https://doi.org/10.5194/hess-17-4769-2013, 2013.

Bloomfield, J. P., Marchant, B. P., McKenzie, A. A., and Lewis, M. A.: Regional analysis of groundwater droughts using hydrograph classification, Hydrol. Earth Syst. Sci., 23, 1397–1416, https://doi.org/10.5194/hess-23-1397-2019, 2019.

Chen, Y., Zhang, Y., Tian, J., Tang, Z., Wang, L., and Yang, X.: Understanding the propagation of meteorological drought to groundwater drought: a case study of the North China Plain, Water, 16, 501, https://doi.org/10.3390/w16030501, 2024.

Ebeling, P., Musolff, A., Kumar, R., Hartmann, A., and Fleckenstein, J. H.: Groundwater head responses to droughts across Germany, Hydrol. Earth Syst. Sci., 29, 2925–2950, https://doi.org/10.5194/hess-29-2925-2025, 2025.

Fiszer, J., and Derkowska-Sitarz, M.: Forecast of development of depression cone and water inflows to brown coal mine Konin, Hydrogeologia, 442, 5–24, 2010.

The Polish Geological Institute - National Research Institute (PGI-NRI): GWB 43 status card, https://www.pgi.gov.pl/dokumenty-pig-pib-all/psh/zadania-psh/jcwpd/jcwpd-40-59/4461-karta-informacyjna-jcwpd-nr-43/file.html, 2022.

Ghasempour, F., Yamaç, S. S., Sekertekin, A., Iban, M. C., and Kutoglu, S. H.: Spatiotemporal agricultural drought assessment and mapping its vulnerability in a semi-arid region exhibiting aridification trends, Agriculture, 15, 2060, https://doi.org/10.3390/agriculture15192060, 2025.

Gleeson, T., Wang-Erlandsson, L., Zipper, S. C., Porkka, M., Jaramillo, F., Gerten, D., and Famiglietti, J. S.: The water planetary boundary, Nature, 588, 257–261, https://doi.org/10.1038/s41586-020-2550-7, 2020.

Goovaerts, P.: Geostatistics for natural resources evaluation, Oxford University Press, Oxford, 1997.

Gorelick, S. M., and Zheng, C.: Global change and the groundwater management challenge, Water Resour. Res., 51, 4409–4438, https://doi.org/10.1002/2015WR017466, 2015.

Guttman, N. B.: Accepting the standardized precipitation index: a calculation algorithm, J. Am. Water Resour. Assoc., 35, 311–322, https://doi.org/10.1111/j.1752-1688.1999.tb03592.x, 1999.

Hengl, T.: A practical guide to geostatistical mapping, European Commission, Luxembourg, 2009.

Hisdal, H., Tallaksen, L. M., and Clausen, B.: Hydrological drought characteristics, in: Drought: a global assessment, edited by: Wilhite, D. A., Routledge, London, 2001.

Jasechko, S.: Global cases of groundwater recovery after interventions, Science, 391, 1218–1228, https://doi.org/10.1126/science.adu1370, 2026.

Jiao, D., Wang, D., and Lv, H.: Effects of human activities on hydrological drought patterns in the Yangtze River, China, Nat. Hazards, 104, 1111–1124, https://doi.org/10.1007/s11069-020-04206-2, 2020.

Jurzyk, K.: Zagrożenie suszą hydrogeologiczną w rejonie JCWPd 43 przy słabym stanie ilościowym wód podziemnych, MSc thesis, University of Warsaw, Warsaw, Poland, 74 pp., 2025.

https://doi.org/10.5194/egusphere-2026-1904
Preprint. Discussion started: 10 June 2026

Kartal, V., and Nones, M.: Assessment of meteorological, hydrological and groundwater drought in the Konya closed basin, Türkiye, Environ. Earth Sci., 83, 285, https://doi.org/10.1007/s12665-024-11587-1, 2024.

Kumar, R., Musuuza, J. L., Van Loon, A. F., Teuling, A. J., Barthel, R., and Broek, J. T.: Multiscale evaluation of the standardized precipitation index, Hydrol. Earth Syst. Sci., 20, 1117–1131, https://doi.org/10.5194/hess-20-1117-2016, 2016.

Ling, Z., Shu, L., Wang, D., Lu, C., and Liu, B.: Assessment and projection of groundwater drought vulnerability under different climate scenarios and land use changes in the Sanjiang Plain, China, J. Hydrol. Reg. Stud., 49, 101498, https://doi.org/10.1016/j.ejrh.2023.101498, 2023.

McKee, T. B., Doesken, N. J., and Kleist, J.: The relationship of drought frequency and duration to time scales, in: Proc. 8th Conf. Applied Climatology, American Meteorological Society, Boston, 179–184, 1993.

Nowak, B., Szadek, P., Szymański, K., and Lawniczak-Malińska, A.: Concept and implementation of solutions improving water relations in the area of the flooded opencast lignite mine Kazimierz Północ (Central-West Poland), Water, 15, 706, https://doi.org/10.3390/w15040706, 2023.

Peters, E., Torfs, P. J. J. F., Van Lanen, H. A. J., and Bier, G.: Propagation of drought through groundwater – a new approach using linear reservoir theory, Hydrol. Earth Syst. Sci., 7, 112–123, https://doi.org/10.5194/hess-7-112-2003, 2003.

Porter, J. R., Xie, L., Challinor, A. J., Cochrane, K., Howden, S. M., Iqbal, M. M., Lobell, D. B., and Travasso, M. I.: Food security and food production systems, in: Climate Change 2014: Impacts, Adaptation, and Vulnerability. Part A: Global and Sectoral Aspects, Cambridge University Press, Cambridge, 485–533, 2014.

Przybyłek, J.: Dewatering problems in lignite mines, Górnictwo Odkrywkowe, 59, 5–14, 2018.

Saha, S., Gogoi, P., Gayen, A., and Chandra, G. P.: Constructing a machine-learning-based spatial drought vulnerability index in Karnataka state of India, J. Clean. Prod., 314, 128073, https://doi.org/10.1016/j.jclepro.2021.128073, 2021.

Sawicka, K., and Jurzyk, K.: Reproducible workflows and processed datasets for groundwater drought vulnerability assessment in GWB 43 (Version 1.0), Zenodo, 2026.

Shukla, S., and Wood, A. W.: Use of a standardized runoff index for characterizing hydrologic drought, Geophys. Res. Lett., 35, L02405, https://doi.org/10.1029/2007GL032487, 2008.

Tallaksen, L. M., and Van Lanen, H. A. J.: Hydrological drought: processes and estimation methods for streamflow and groundwater, Elsevier, Amsterdam, 2004.

Teutschbein, C., Grabs, T., Giese, M., Todorović, A., and Barthel, R.: Drought propagation in high-latitude catchments: insights from a 60-year analysis using standardized indices, Nat. Hazards Earth Syst. Sci., 25, 2541–2564, https://doi.org/10.5194/nhess-25-2541-2025, 2025.

Thomas, B. F., and Famiglietti, J. S.: Groundwater depletion, Geophys. Res. Lett., 44, 11445–11455, https://doi.org/10.1002/2017GL075965, 2017.

Van Loon, A. F.: Hydrological drought explained, WIREs Water, 2, 359–392, https://doi.org/10.1002/wat2.1085, 2015.

Van Loon, A. F., Stahl, K., Di Baldassarre, G., Clark, J., Rangecroft, S., Wanders, N., Gleeson, T., Van Dijk, A. I. J. M., Tallaksen, L. M., Hannaford, J., Uijlenhoet, R., Teuling, A. J., Hannah, D. M., Sheffield, J., Svoboda, M., Verbeiren, B.,

https://doi.org/10.5194/egusphere-2026-1904
Preprint. Discussion started: 10 June 2026

Wagener, T., and Van Lanen, H. A. J.: Drought in a human-modified world: reframing drought definitions, understanding, and analysis approaches, Hydrol. Earth Syst. Sci., 20, 3631–3650, https://doi.org/10.5194/hess-20-3631-2016, 2016.

Vega Briones, J., Sutanudjaja, E. H., de Jong, S., and Wanders, N.: Modelling groundwater hydrological drought and its recovery given natural and anthropogenic scenarios in South America, Hydrol. Process., 38, e15340, https://doi.org/10.1002/hyp.15340, 2024.

Vicente-Serrano, S. M., Beguería, S., and López-Moreno, J. I.: A multiscalar drought index sensitive to global warming: the standardized precipitation evapotranspiration index, J. Climate, 23, 1696–1718, https://doi.org/10.1175/2009JCLI2909.1, 2010.

Wheater, H. S., and Evans, E. J.: Land use and flood risk, Land Use Policy, 26, S251–S264, https://doi.org/10.1016/j.landusepol.2009.08.007, 2009.

World Meteorological Organization: Standardized precipitation index user guide (WMO-No. 1090), WMO, Geneva, 2012.

Zhu, R., Zheng, H., and Jakeman, A. J.: Groundwater drought variability and its propagation, Water Resour. Res., 58, e2021WR030841, https://doi.org/10.1029/2021WR030841, 2022.